Assessing the spatial variability of snow and sea ice properties with different spatial analytical approaches

Bachelor thesis in the bachelor degree course

Physical Geography

Friedrich-Alexander-University Erlangen-Nürnberg
Institute of Geography (FAU)

in cooperation with
Alfred-Wegener-Institute, Bremerhaven (AWI)

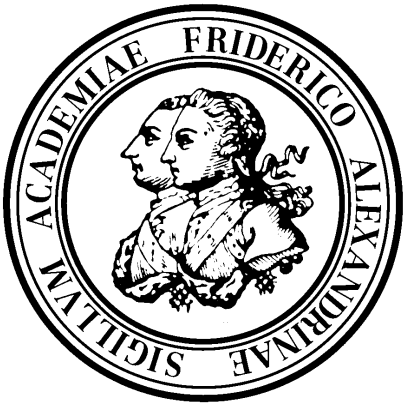

Svenja Annika Rudolph

supervisor: Prof. Dr. Matthias Braun (FAU)

co-supervisors: Benjamin Lange (AWI), Dr. Hauke Flores (AWI)

Erlangen, 2016

Table of contents

List of Tables

List of Figures

Chapter 1

Introduction

Large scaled calculations by The Cryosphere Today (2016) show that the extension and thickness distribution of sea ice follows a downward trend in all months since 1978. It reaches its annual minimum near the end of September and its annual maximum around the end of March (Stroeve et al., 2012; Cassano et al., 2013). Miles et al. (2014) calculated a mean sea ice extent decline rate of $0.40x106km^2(10yr)^{-1}[or3$

By September 2016 it is likely there will be a new record minimum sea ice extent. This development has also a high impact on the Arctic marine ecosystem (Lange, 2016). Lange (2016) demonstrated that springtime biomass of MYI may be largely underestimated with further implications to Arctic-wide ecosystems. As a given example Katlein et al. (2014) and Lange (2016) observed a relatively high biomass of under-ice algal aggregates and in-ice-algal in regions, which are dominated by MYI, in comparison to FYI dominated areas. To get a better knowledge about the physiological conditions of this part of the sea ice ecology system, it is necessary to find out how much they are controlled by physical sea ice properties such as its thickness and snow cover. Lange (2016) used light extinction coefficients, as a function of the snow and the sea ice thickness (chapter 2.2), as a proxy for sea ice algae habitat to identify spots on the sea ice with a high potential for bottom-ice algal growth. Since the light extinction coefficient is correlated to the amount of snow and the ice thickness, it might be useful to estimate the spatial distribution of sea ice habitats over a larger area by using interpolation that can extrapolate the characteristic variability of snow and ice thickness on MYI and on FYI.

There is a huge field of different statistical and non-statistical interpolation methods to solve this problem such as Inverse Distance Weightning (non-statistical), Kriging (statistical) or the Polygon method (non-statistical). Ordinary Kriging is a popular and commonly used geostatistical method to explain spatial variability of three dimensional data and therefore was chosen to try to solve the given problem. This does not mean that other methods could be used instead as good as or better as Ordinary Kriging.

The objective of this study is to show if and how the geostatistical method Ordinary Kriging – implemented in R and performed by using the Exponential model and a hole-effect model - can be used to interpolate the snow and the ice thickness of a FYI floe

and a MYI floe. The fitting of this method shall capture the actual pattern of the data in any direction and shall satisfactorily produce a realistic snow and sea ice matrix in three dimensions, which also accurately captures important features of the sea ice such as hummocks, snow drift patterns and interconnected melt pond systems. The second aim is to investigate the spatial distribution of the physical properties and try to lead them to observed relationships between these properties.

Chapter 2 gives a brief overview of the origin of the data in its first subsection. The second subsection, methods, explains the principle of Ordinary Kriging and its theoretical background.

Chapter 3 deals with the results. First the distribution of the snow and sea ice thicknesses within the transects of both stations will be described. The following subsection focusses on the interpolated spatial distribution of the snow and sea ice properties. The last two chapters focus on how we parameterized the Ordinary Kriging and its variograms, and compare the performance of the two different models.

Chapter 4 summarizes and discusses briefly the final outcomes of the study and gives a short conclusion.

Chapter 2

Data and methods

2.1 Data

The data used for this study were sampled during early May 2013 on sea ice located within the Lincoln Sea, north of Ellesmere Island, Nunavut, Canada (Figure 2.1; Lange, 2016). Station A2 was measured on a FYI floe and station A6 was sampled on a MYI floe. The electromagnetic (EM) thickness of the snow and the ice were performed by using the EMP-400 from GSSI (Lange, 2016). A more detailed description of the data sampling and processing of sea ice freeboard, sea ice thickness and snow thickness over two perpendicular transects, which cross in the middle, can be found in Lange (2016). The Bulk integrated light extinction coefficient, in this study named as Bulk k, was calculated from Lange (2016) as a function of the light extinction coefficients (m^{-1}) for ice and snow by the given equation:

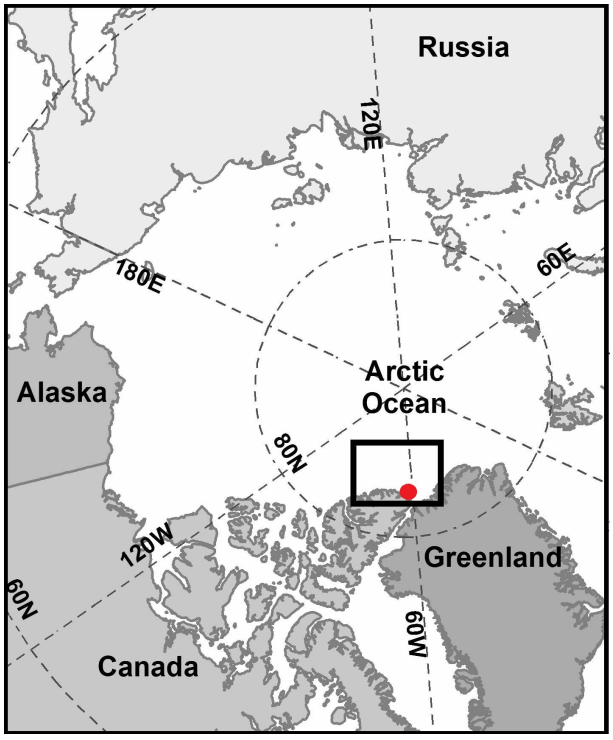

Figure 2.1: Overview map of the data location (modified by the author and taken from Lange, 2016)

$$k_B = (snow_i * 20) + (ice_i * 1.55) \tag{2.1}$$

where $snow_i$ is the given thickness of the snow and ice_i the given thickness of the ice at particular location i . The snow and ice thickness parameter were transformed to a measurement scale of cm to provide a uniform usage of thickness units.

2.2 Spatial Analyses

The interpolation was performed by using Ordinary Kriging. The following subsections will give an introduction to Kriging theory in general and to the Ordinary Kriging with the models used for these thesis.

2.2.1 Kriging

Kriging is a geostatistical method based on the ansatz, that the Euclidian distance and the direction between two reference points do reflect a dependency (Deutsch & Journel, 1998). It explains the observed variability of surfaces (Schabenberger & Gotway, 2005), such as sea ice or snow. As a statistical and mathematical basis for Ordinary Kriging analyses, the theoretical and the experimental (i.e., empirical) variograms are necessary. They are described in the following subsection.
Kriging is named after the South-African mining engineer D.G. Krige, who developed the first steps of the Kriging theory (Deutsch & Journel, 1998) and G. Matheron further developed upon this theory in the middle of the 20th century (Deutsch & Journel, 1998). It is a best linear unbiased estimator (BLUE) that provides an unbiased estimation at locations with unknown values (Deutsch & Journel, 1998). There are three different main methods of Kriging: Simple Kriging, Ordinary Kriging and Universal Kriging. Simple Kriging assumes, that the constant mean of the observed values is known (Montero & Mateu, 2015). Since this is often unknown, this method is rarely used (Schabenberger & Gotway, 2005). Conversely, Ordinary Kriging assumes that the constant mean of the observed values is unknown (Montero & Mateu, 2015) and Universal Kriging, as being an extension of Ordinary Kriging, provides additionally a supplementary estimation of trends in the data. This is considered in the Kriging as a modelled polynomial (Montero & Mateu, 2015). Since Ordinary Kriging is used in this thesis, it will be explained in more detail in the following subsections.

2.2.2 The Variogram

The variogram is the foundation of Ordinary Kriging and describes the spatial variability between the given data points referring to their Euclidian distance (i.e., lag distance). It is based on two different models: the experimental (i.e., empirical) variogram and the theoretical variogram. The experimental variogram estimates for each distance h a value for the variogram by using the classical variogram estimator for the distance vertices of the observed values (Journel & Huikbregts, 1978). The values are classified afterwards and divided into distance- and direction classes to estimate the distance vertices without known observation values (Journel & Huikbregts, 1978) and is established in a geostatistical model. The observed values $z(u_1), \ldots, z(u_n)$ at the observed locations $u_1, \ldots, u_n$ are used as realisations of random variables $Z(u_1), \ldots, Z(u_n)$ and locations with unknown values are also regarded as random values (Deutsch & Journel, 1998).

The sum of both are defined as a random function or the stochastic process (Deutsch & Journel, 1998).

Within the model, the spatial relationship between the random values is defined by their Euclidian distance and their direction (Deutsch & Journel, 1998). This property of the model is described as an intrinsic stationary process if the estimation value of all random values is equal (Deutsch & Journel, 1998)

$$E[Z(u)] = \mu \tag{2.2}$$

and the spatial relationship is not dependent on the present localization but on the distance vertices u and v in the study area (Robinson & Metternicht, 2006):

$$Zus[Z(u), Z(v)] = \gamma(h) \tag{2.3}$$

$$h = v - u \tag{2.4}$$

The variance of the difference between these two data values is used and defines their distance vertices as (Deutsch & Journel, 1998):

$$\gamma(h) = Var[Z(u) - Z(u+h)] \tag{2.5}$$

In theory, the variogram is expected to grow continuously with its lag distance, which means the larger the lag distance the less the relationship between two variables and therefore the higher the variance of its difference (Deutsch & Journel, 1998).

The experimental variogram is the foundation of the theoretical variogram that needs to be established afterwards. The theoretical variogram is built up on a mathematical function, where its progress is known respectively can be predicted. They have to be conditional negative semidefinite (Deutsch & Journel, 1998), but Pyrcz & Deutsch (2003) pointed out that in case of using a hole-effect model the covariance pendant of the theoretical variogram has to be positive definite.

Commonly used functions, which accomplish these requirements, are the Gaußian model, the Spherical model, the Matern model, the Stein-Matern model, the Exponential model and the Linear model (Deutsch & Journel, 1998; Schabenberger & Gotway, 2005; Montero & Mateu, 2015). As it will be shown in chapter 3.3, the experimental variograms do not show an expected monotonic growth. Therefore we decided to compare for this thesis the Exponential model

$$\gamma(h) = c * (1 - \exp(\frac{-3h}{a})) \tag{2.6}$$

where h is the lag distance, a is the range and c the sill, with a hole-effect model, the Wave model (Deutsch & Journel, 1998; Schabenberger & Gotway, 2005; Montero & Mateu, 2015):

$$\gamma(h) = (\frac{a}{h}) \sin \frac{h}{a} \tag{2.7}$$

The progress of those functions within the previously established experimental variogram is controlled by three parameters: Sill, nugget and range. The setting of these three parameters shall reflect the pattern of the experimental variogram as good as possible (Deutsch & Journel, 1998).The sill of the variogram is in theory defined as the semivariance value, where the variogram levels off (Schabenberger & Gotway, 2005; Deutsch & Journel, 1998; Montero & Mateu, 2015). Based on other studies (Das, Rao, & Boshnakov, 2012; Sajid,Rudra & Parkin, 2013), the sill values were always calculated as the squared standard deviation (i.e., variance) of each property for this study. The nugget is defined to represent the variability of values with smaller distances rather than the common overall variability (Schabenberger & Gotway, 2005). It is common to set the nugget values by using the given value of the (semi-)variogram at the first lag interval (Sajid,Rudra & Parkin, 2013; Schabenberger & Gotway, 2005; Montero & Mateu, 2015). This solution was also used in this study. The range describes the scale of the distance, where the semivariogram reaches the sill and can also be interpreted as the patch size of the property (Schabenberger & Gotway, 2005). This definition was used for estimating the range of the Exponential model. Since there are only a few studies published, which use and parameterize the Wave model (e.g. Das, Subba Rao & Boshnakov, 2012) the range for this model was estimated by following the instructions of Pyrcz & Deutsch (2003) to reproduce the observed hole-effect structures in the variograms. So for estimating those ranges the distances to the first peaks and the dampening factors were considered. It is supposed to result in a modelled amplitude that is almost equal to the original amplitude of the experimental variogram.

In summary it can be said that the aim of the fitted theoretical variogram is to build a spatial relationship between a value patter, whose progress is not described by a mathematical function, represented by the experimental variogram, and a value patter, whose progress can be described by a mathematical function and their parameterization, represented by the theoretical variogram.

2.2.3 Ordinary Kriging

The Krige estimator $z*(u_0)$ is defined in Deutsch & Journel (1998) as

$$z*(u_0) = \sum v_i, z(u_i) \tag{2.8}$$

with its determination of the weights for the given point u_0 by solving the extremum problem:

$$E[F(u_0)] = 0 \tag{2.9}$$

with its secondary condition, the Kriging variance

$$Var[F(u_0)] = min\,\{F(u_0), v_1, ..., v_n\; real\; numbers\} \tag{2.10}$$

where $F(u_0)$ is the estimation error, which is zero on average. This second condition requires the error estimate has minimal variance (Deutsch & Journel, 1998). The linearity of the estimation value and the stationarity of the process can be simplify the Kriging variance by the following equation (Deutsch & Journel, 1998):

$$0 = E[F(u_0)] = E[Z(u_0) - \sum v_i \, Z(u_i)] \tag{2.11}$$

$$0 = E[Z(u_0] - (\sum v_i E[Z(u_i)]) = E[Z(u_0)](1 - \sum v_i) \tag{2.12}$$

which sums the weights up to one and define the variance of the error estimate as (Deutsch & Journel, 1998):

$$1 = \sum v_i \tag{2.13}$$

The equation is solved by using system of linear equations, the Lagrange multiplier (Deutsch & Journel, 1998; Schabenberger & Gotway, 2005). The solution value is the weight of the estimator and has to be calculated for each value that needs to be estimated (Deutsch & Journel, 1998):

$$\sum v_j \gamma(u_i - u_j) + \nu = \gamma(u_i - u_0) \tag{2.14}$$

$$1 = \sum v_i \tag{2.15}$$

$$\begin{bmatrix} \gamma_{11} & \dots & \gamma_{1n} & 1 \\ \dots & \dots & \dots & \dots \\ \gamma_{n1} & \dots & \gamma_{nn} & 1 \\ 1 & \dots & 1 & 0 \end{bmatrix} = \begin{bmatrix} v_1 \\ \dots \\ v_n \\ v \end{bmatrix} = \begin{bmatrix} \gamma_{10} \\ \dots \\ \gamma_{n1} \\ 1 \end{bmatrix} \tag{2.16}$$

$$C \cdot v = D \tag{2.17}$$

Where v is an auxiliary variable from the Lagrange multiplier and $i = 1, \dots n$. Its solution is:

$$v = C^{-1} D \tag{2.18}$$

Because γ is definite, the matrix C is thus invertible (Deutsch & Journel, 1998). This is giving the weights of the Krige estimator for the location u_0. Therefore the estimation value is defined as (Deutsch & Journel, 1998):

$$z*(u_0) := \sum v_i z(u_i) \tag{2.19}$$

Matrix D consists of the variogram values between the estimated value and the neighboured values that are considered for the estimation (Deutsch & Journel, 1998). This describes the relationship between these values (Deutsch & Journel, 1998). Kriging fits the weights to the real prediction by using the Euclidian distance instead of using the variogram values (Deutsch & Journel, 1998). Matrix C sums up the variogram values between all values that are neighboured to the estimated value (Deutsch & Journel, 1998). This means that two values with a close distance will result in a low variogram value and

vice versa.

$$weights(v) = cluster(C^{-1}) * distance(D) \tag{2.20}$$

Multiplying the matrices C and D catches the clusters of the neighboured points. It reduces the weight of close points, and distribute them to other values in the neighbourhood (Deutsch & Journel, 1998). This produces the dependence between the Euclidian distance and the direction between two reference points (Deutsch & Journel, 1998). The Kriging variance is the variance of the error estimate and describe the configuration of the grid (Schabenberger & Gotway, 2005). The (semi-)variograms have a large influence on the Kriging variance, e.g. a high range of the theoretical function reduces the Kriging variance and vice versa (Schabenberger & Gotway, 2005; Deutsch & Journel, 1998).

Chapter 3

Results

3.1 Site description

3.1.1 Station A2

All observed properties at station A2 were characteristic to First-Year sea ice (FYI) regarding their measures of dispersion, presented in Table 3.1 (chapter 3.2), and the snow and sea ice profiles in Figure 3.1 (Thomas & Dieckmann, 2009). The range of values show a relatively uniform distribution for the sea ice thickness (IQR: 169-180 cm) and ice cm) and ice freeboard (IQR: 10-14 cm). This can be confirmed by the profiles in both directions (Figure 3.1). However, the variability of snow might has a higher variability (IQR: 10-23 cm) and by looking at the profiles the amount of snow is slightly less in the south-north direction than it is observed in the east-west profile and varies in its surface topography more than the sea ice freeboard. Since the measurements cover a distance of 100 m in each direction, it can be assumed that these variations are caused by small scale snow drifts. There is a negative correlation between the snow thickness and the total ice thickness regarding to its overall distribution (Lange 2016). This is the result of increased thermal insulation in regions of thicker snow, which thus limits sea ice growth by reducing the heat flux between ocean, sea ice and the atmosphere.

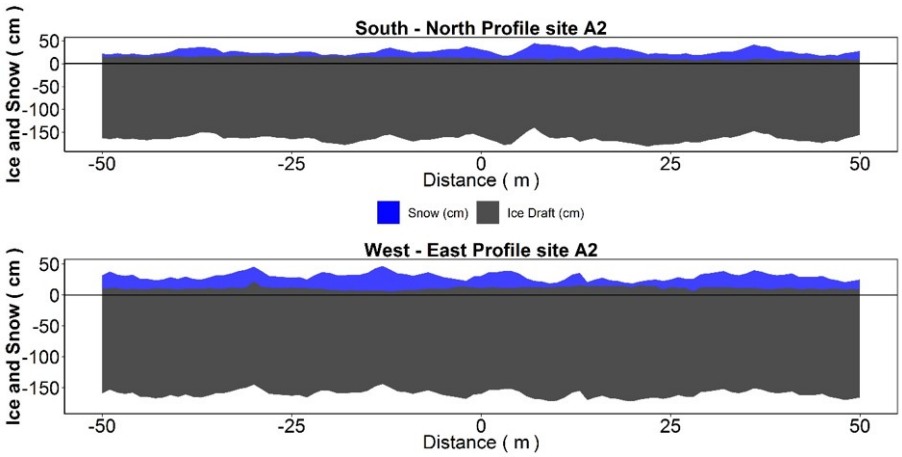

Figure 3.1: : Distribution of the measurements at Station A2 as vertical profiles (modified by the author; taken from Lange, 2016).

3.1.2 Station A6

The summary of snow and ice properties from station A6 are presented in Table 3.1. The corresponding profiles in S-N direction and E-W direction for A6 are shown in Figure 3.2. Both profiles show characteristic properties of Multi-Year sea ice (MYI; Thomas & Dieckmann, 2009). For one, the overall thickness of snow depth is thicker than the FYI site A2, Furthermore, the spatial distribution of the snow and ice thickness much more variable than FYI site A2 (Figure 3.1 and Figure 3.2). By choosing the mean and maximum sea ice thickness and correlating it to a typical timescale of growth by Eicken and Petrich (2009), the MYI is estimated to have an age of approximately 2 – 2.5 years. All observed snow and ice surface properties have highly undulating patterns. The bottom of the sea ice also shows a high varying under-ice topography.

The deepest accumulations of snow can be observed close to the intersection of the two transects (i.e., at the centre of the cross; Figure 3.2). In this area, the weight of the snow pushes the sea ice below the sea level, which results in negative measurements of the sea ice freeboard. For comparison, the total sea ice thickness in this area decreases to the median level, 175 cm, of the sea ice thickness at station A2. This combination of the snow and sea ice properties may indicate the presence of a melt pond in the former summer(s), which resulted in reduced sea ice thickness by two processes. First, it can be assumed that the low albedo of the melt pond increased the solar transmittance and absorption of solar radiation by the sea ice, which enhanced melt in the melt pond regions during summer. Second, the high amount of snow that accumulated over winter and into springs in these low topographic regions by precipitation, drift and transport processes resulted in limited sea ice growth due to thermal insulation, as described for the FYI. Its effect of thermal insulation limits the growth of sea ice to a thinner level compared to adjacent regions with thinner or no snow cover. Many similar features, which could represent melt ponds, were observed by looking at the profiles (Figure 3.2).

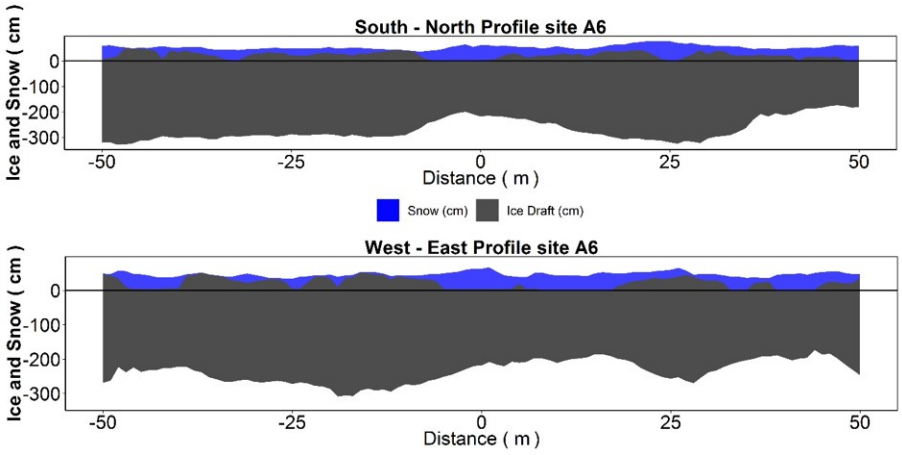

Figure 3.2: : Distribution of the measurements at Station A6 as vertical profiles (modified by the author; taken from Lange, 2016).

Since these profiles give only a two dimensional overview, we assumed that the sea ice surface topography shows a cross-section of an interconnected network of melt ponds, which formed and grew during the previous summers.

3.2 Spatial variability of the snow and sea ice properties

Ordinary Kriging with the Wave model produced a spatial distribution that estimates the in-situ variability and patch-size of the properties more reliably and realistically than the exponential model (Figure 3.4 - Figure 3.9). From the Wave model it is possible to identify and to validate observations that were made on the two-dimensional profile in the previous chapter. Therefore the following subsections discuss the observations of the snow and sea ice properties that were made by looking at the outcome of the Wave model. The statistical summary of the ice thickness distribution is shown in Table 3.1 for each station, model and property.

3.2.1 Snow thickness at Station A2

The snow thickness of the Wave model at station A2 varies between 6,74 cm and 28,45 cm and has a mean thickness of 15,83 (Table 3.1). This is a smaller range of values than the observed snow thicknesses, which shows a maximum snow thickness of 40 cm. This might be caused by how the performance of the interpolation was set. The parameterization is described in chapter 2.2.1. The IQR of the wave model prediction is 3,66 cm (Table 3.1), which indicates that the snow thickness has a relatively uniform distribution, but by looking at the spatial distribution of all given data points on the map (Figure 3.5), some general patterns are apparent that may be interpreted as transport processes. On and close to the data point axes, three little snow drifts were identified (Figure 3.5). The highest one is located close to the centre of map (Figure 3.5). They are interpreted to be accumulation deposits formed by precipitation and wind transport processes. We assume that the snow drift close to the centre of the map was interpolated with a higher elevation value, because the closer Euclidian distances from the data points resulted in a higher estimation accuracy than in case of the two snow drifts on the outer East-West axis. Beyond that we assume that the snow drift in the very east of the map is connected with the drift in the centre, because the observed and the interpolated values in the area between these two features differ only slightly (Figure 3.5). The overall interpolated surface of the Wave model does not reflect the real in-situ situation, but is giving some clues, which are supported by the observed data values. Regarding to the spatial scale of all observations, measured and interpolated, it might be possible that the snow surface shows a large system of snow drifts and valleys, which do group into areas with a higher amount of snow drifts and areas with less amount of snow accumulation. This drifting wave-like pattern can be linked primarily to snow accumulation and transport processes by wind coming probably from one direction since snow drifts typically form perpendicular to the wind direction (e.g., Gosselin et al., 1988). Figure 3.3 shows a sketch of this assumed overall distribution based on results from the Ordinary Kriging analyses. Since snow thickness and distribution varies on shorter time scales than sea ice, because of its

Table 3.1: Statistical summary of the results divided by Models (Mdl) = observed (obs), wave (WAV), exponential (EXP); station (ST) = A2, A6; Property (P) = Bulk K (BK), sea ice (I), snow (S), sea ice freeboard (IF); Minimum value (Min), Interquartile range (IQR), maximum (Max)

ST	**P**	**Mdl**	**Min**	**IQR**	**Max**	**ArM**	**SSE**	**BIAS**	**RMSE**	**N**
A2	BK	Obs	3,587	2,24	10	6,136				201
A2	I	Obs	150,5	11,3	192,7	174,4				201
A2	S	Obs	3	12,5	40	17,17				201
A2	IF	Obs	6	4	22	11,78				201
A6	BK	Obs	4,587	4,142	20	10,077				201
A6	I	Obs	175	96,1	379	275,2				201
A6	S	Obs	0,5	25	75	29,06				201
A6	IF	Obs	-4	30	52	21,95				201
A2	BK	Exp	3,677	0,326	10,013	6,059	41,9939	0,0581	0,6804	10609
A2	I	Exp	152,2	1,4	192	174,2	1599,503	-0,6262	4,6009	10609
A2	S	Exp	3,508	1,647	38,309	16,807	1253,21	0,3367	3,7271	10609
A2	IF	Exp	7,083	2,798	16,978	11,465	250,0146	-0,1726	1,3519	10609
A2	BK	Wav	4,106	0,904	8,341	6,032	126,8017	0,1637	1,0412	10609
A2	I	Wav	161,3	4,1	187,3	174,7	4235,636	-0,7364	6,2211	10609
A2	S	Wav	6,101	4,818	29,074	16,572	3728,474	0,8752	5,6202	10609
A2	IF	Wav	8,726	2,442	16,912	11,887	308,866	-0,0072	1,6362	10609
A6	BK	Exp	4,704	0,205	18,49	10,044	352,007	0,1312	1,6048	10609
A6	I	Exp	177	35	369,3	276,3	26949,1	-1,6701	14,4356	10609
A6	S	Exp	1,008	1,753	67,127	28,721	10937,69	0,7176	8,7549	10609
A6	IF	Exp	-1,791	0,655	49,136	22,336	9883,06	-0,4287	8,1103	10609
A6	BK	Wav	4,982	1,178	15,236	10,014	478,9805	0,191	2,1923	10609
A6	I	Wav	178,2	35	353,8	279,2	41806,55	0,3033	21,0402	10609
A6	S	Wav	-2,734	6,857	52,79	29,259	14972,81	1,3145	11,746	10609
A6	IF	Wav	0,3079	6,7138	43,6457	22,0338	14527,3	0,3748	10,9941	10609

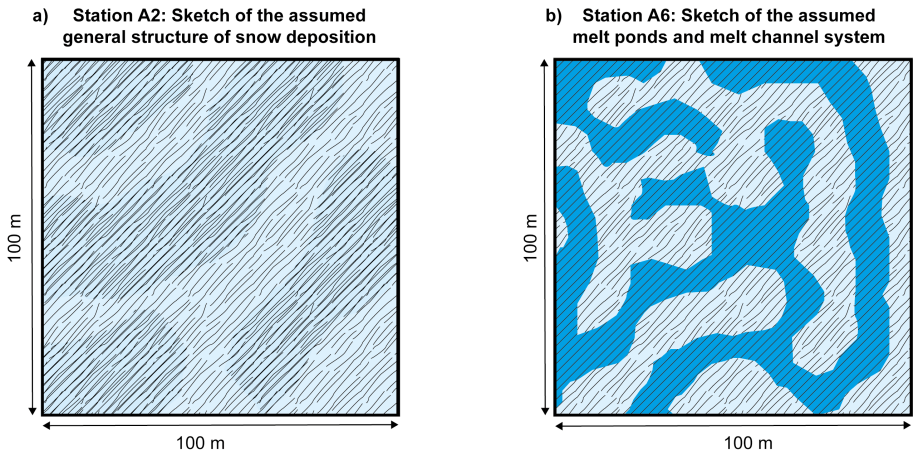

Figure 3.3: : Sketches of the assumed overall surface structures.

high sensitivity to atmospheric related processes such as solar radiation or wind (Rösel et al., 2012), this pattern is only a snapshot and may be a representation of the overall long-term processes of snow accumulation and re-distribution.

3.2.2 Snow thickness at Station A6

The snow thickness of the Wave model at station A6 varies between 4.4 cm and 54,4 cm and has a mean thickness of 29 cm (Table 3.1). Similar to station A2, this is also a smaller range than the observed range, which shows a maximum snow thickness of 75 cm and is also interpreted to be caused by how the theoretical semivariogram of the interpolation was set. The IQR of the wave model prediction is 5,1 cm (Table 3.1), which may also indicate that the snow thickness has a uniform distribution similar to station A2. However, it is likely that this model does not reflect the real in-situ situation of the surface, but may still provide some clues, which can be supported by the observed data values. The spatial distribution of all given data points on the map (Figure 3.8), can be linked to different processes of snow and sea ice morphology. The surface map shows a highly undulating and hummocky topography (Figure 3.8). These bumps and troughs spread out on larger distances of the grid form an interconnected network of snow and sea ice features. In chapter 3.1 we suggest, that the highly undulating surface with interconnected features could be interpreted as the result of a refrozen melt water accumulation network from previous summer(s). The interpolated surface of the snow thickness supports this assumption and therefore these bumps and troughs are interpreted to be snow packs that fill up a refrozen melt pond or melt channel. The dimensions of the shown channelized topography could fit to the real dimensions of interconnected melt pond systems (Rösel et al., 2012). Figure 3.3 shows a sketch with an assumption of the spatial distribution from an interconnected channel system, based on the Kriging result from the snow thickness and the thickness of the sea ice freeboard.

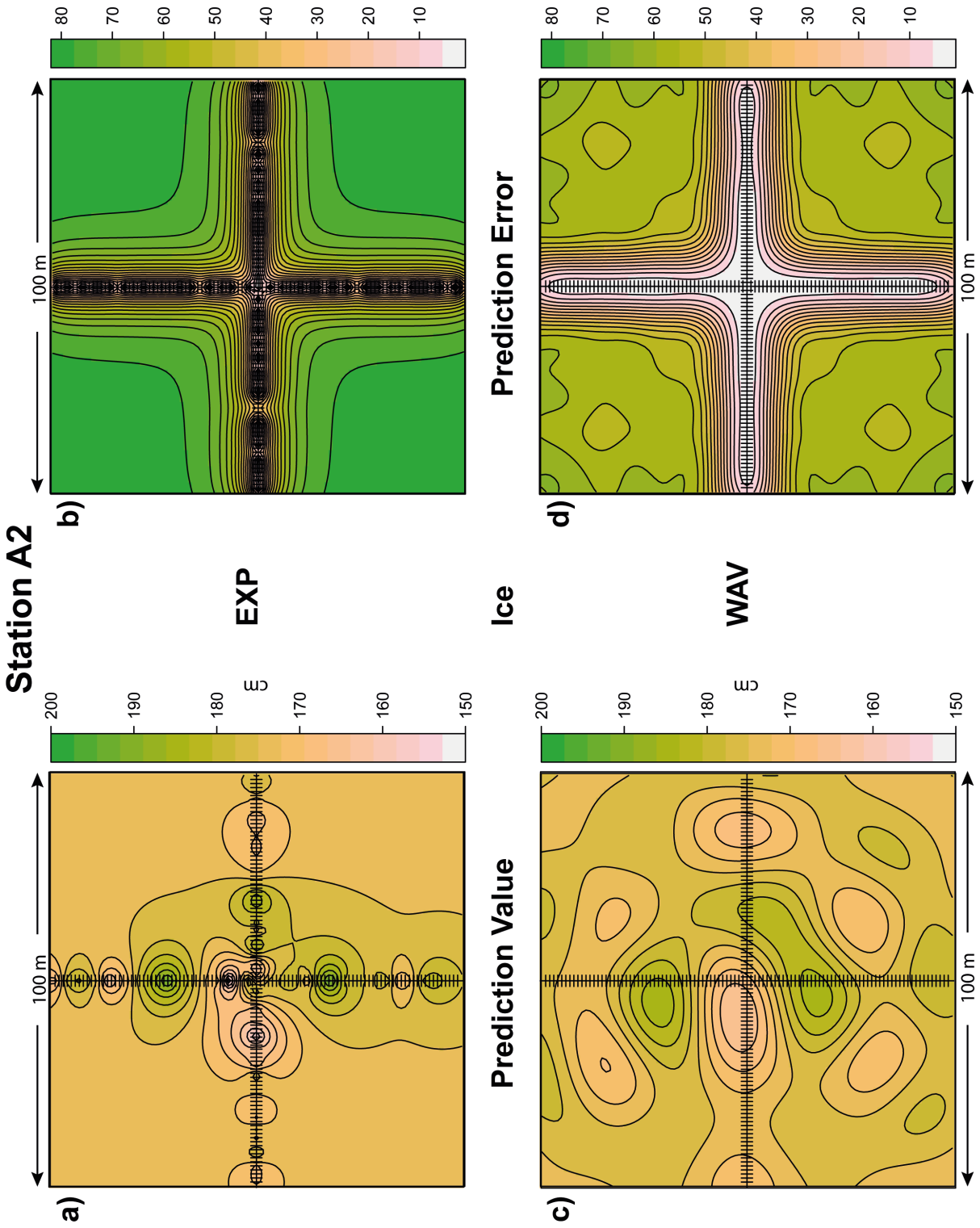

Figure 3.4: Maps with Ordinary Kriging results for sea ice at station A2: a) Exponential model predicted value, b) Exponential model predicted error, c) Wave model predicted value, d) Wave model predicted error.

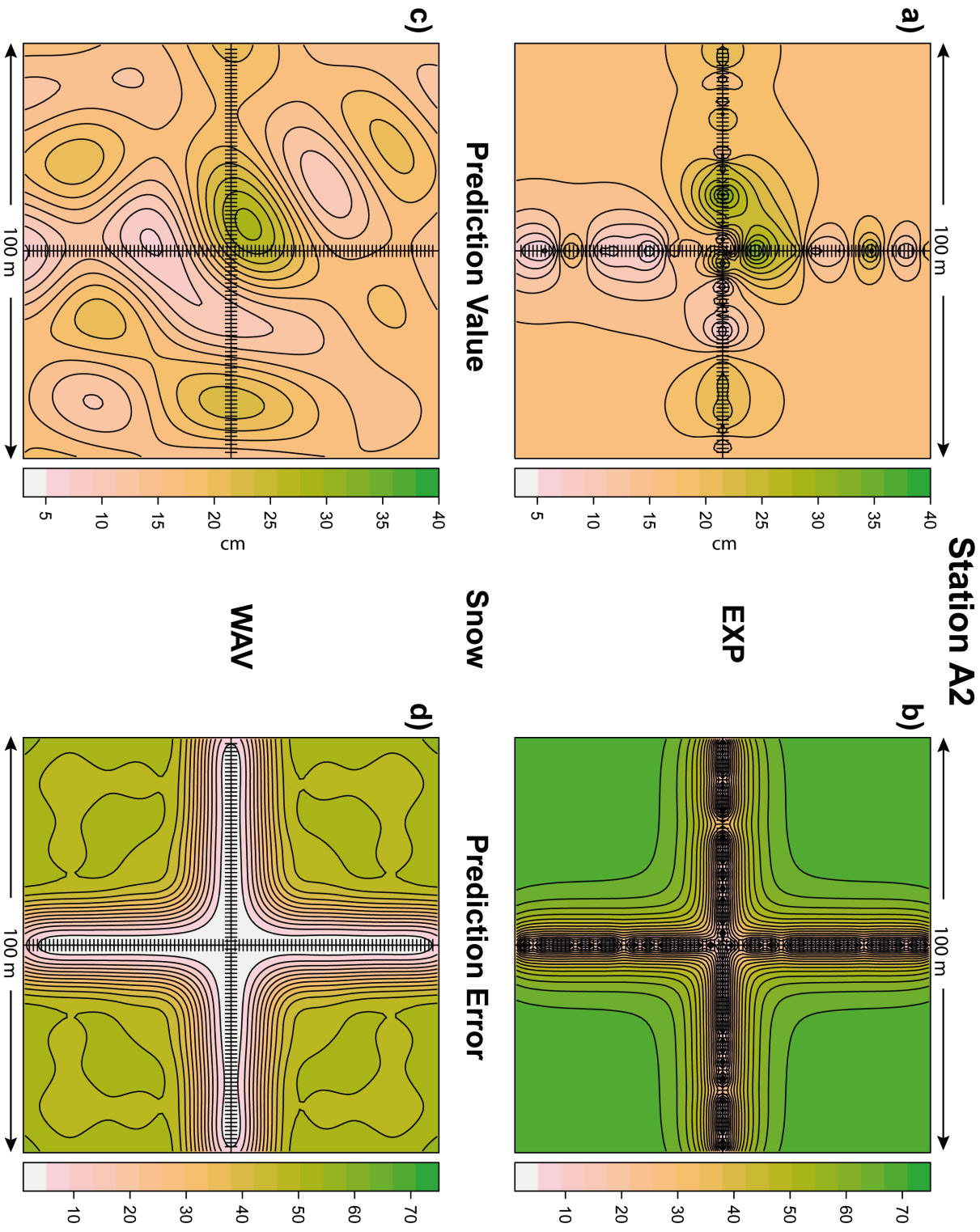

Figure 3.5: Maps with Ordinary Kriging results for snow at station A2: a) Exponential model predicted value, b) Exponential model predicted error, c) Wave model predicted value, d) Wave model predicted error.

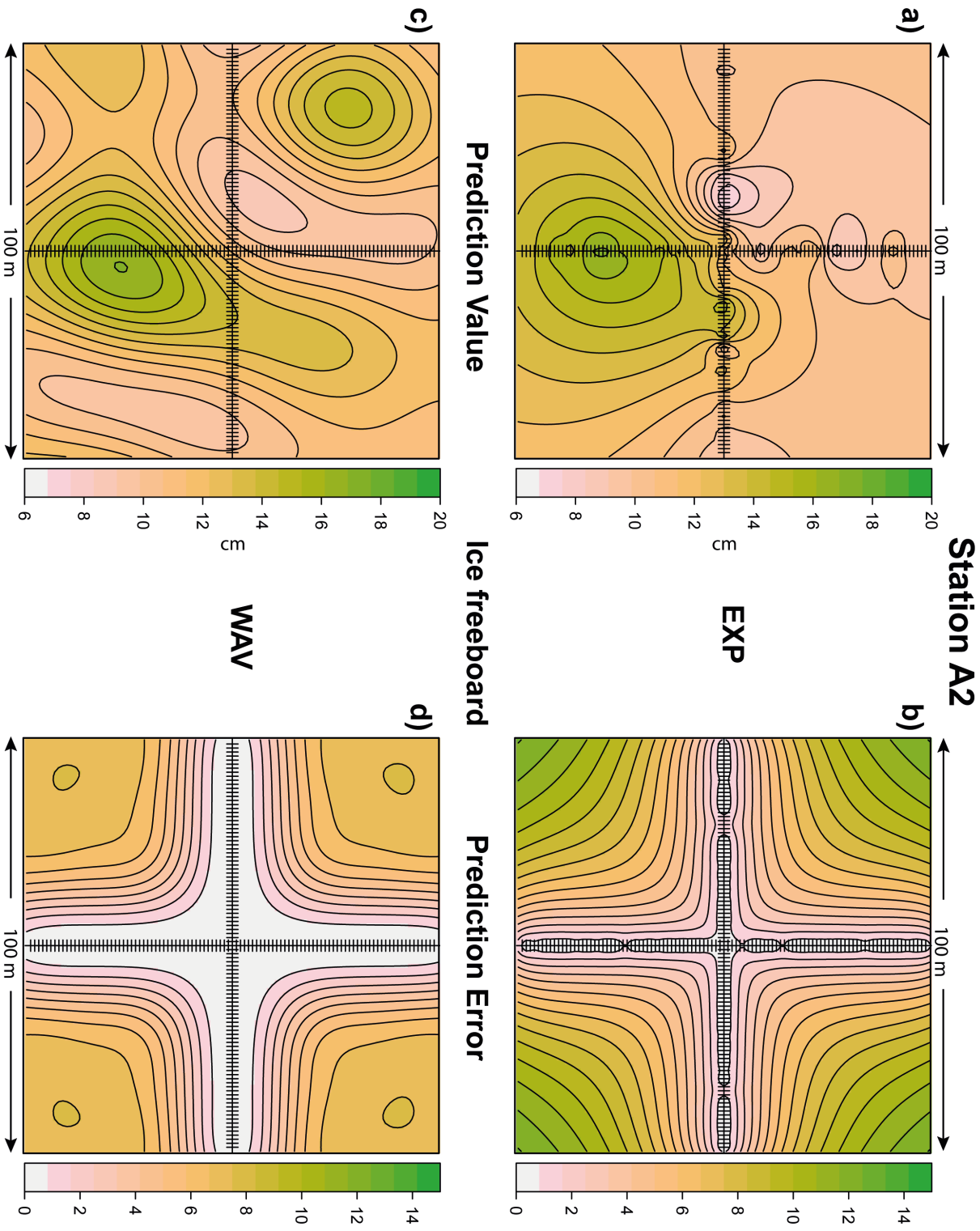

Figure 3.6: Maps with Ordinary Kriging results for sea ice freeboard at station A2: a) Exponential model predicted value, b) Exponential model predicted error, c) Wave model predicted value, d) Wave model predicted error.

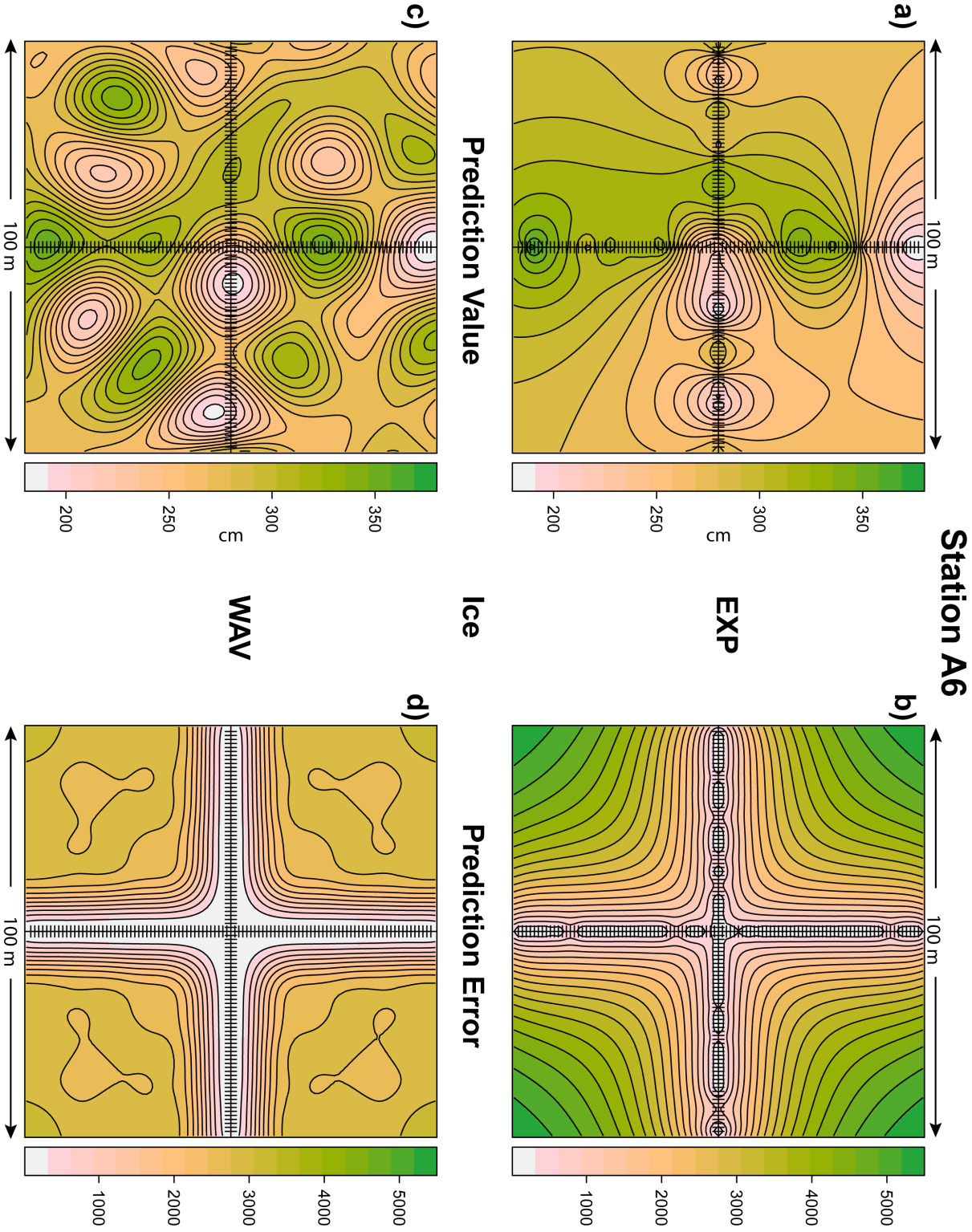

Figure 3.7: Maps with Ordinary Kriging results for sea ice at station A6: a) Exponential model predicted value, b) Exponential model predicted error, c) Wave model predicted value, d) Wave model predicted error.

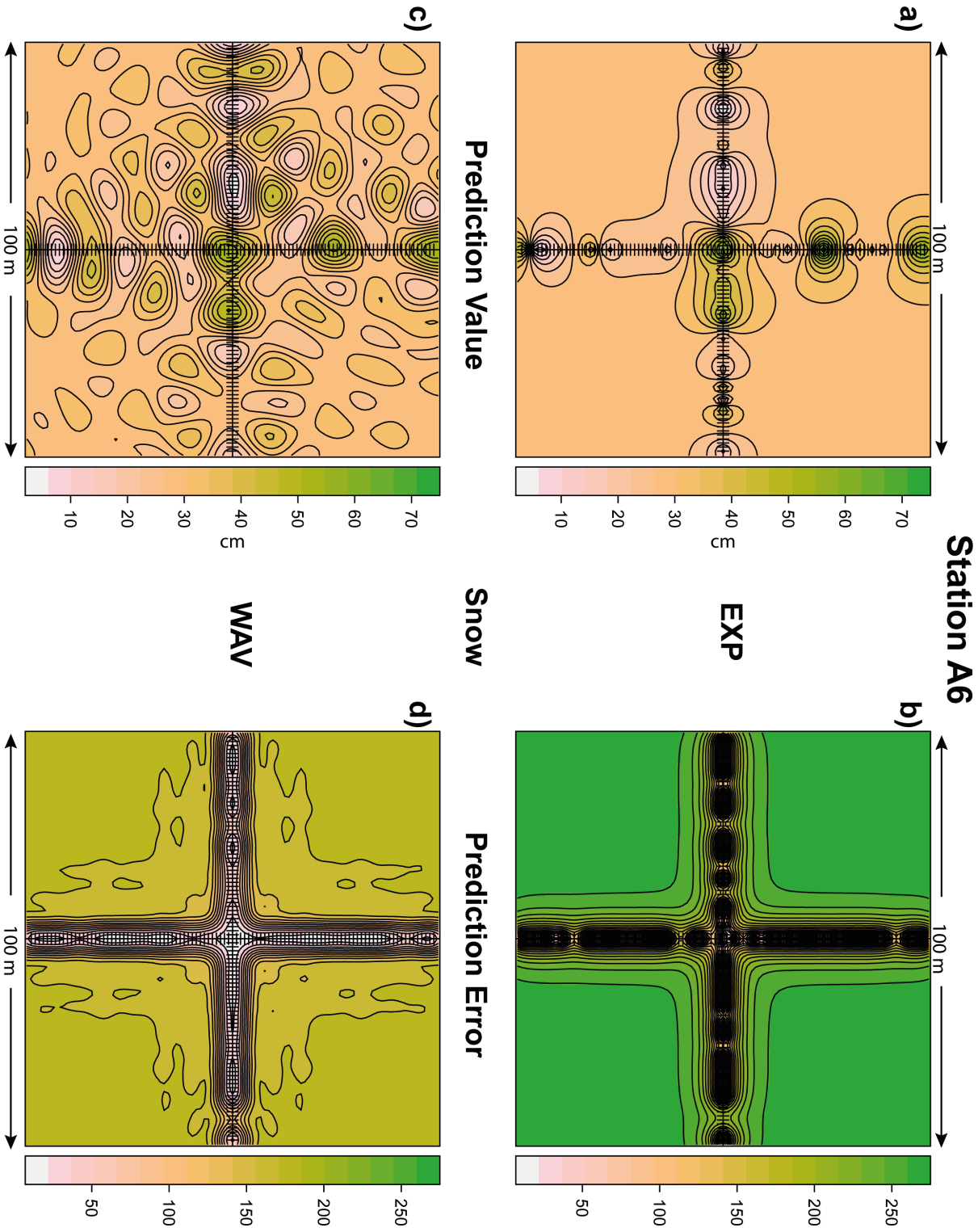

Figure 3.8: Maps with Ordinary Kriging results for snow at station A6: a) Exponential model predicted value, b) Exponential model predicted error, c) Wave model predicted value, d) Wave model predicted error.

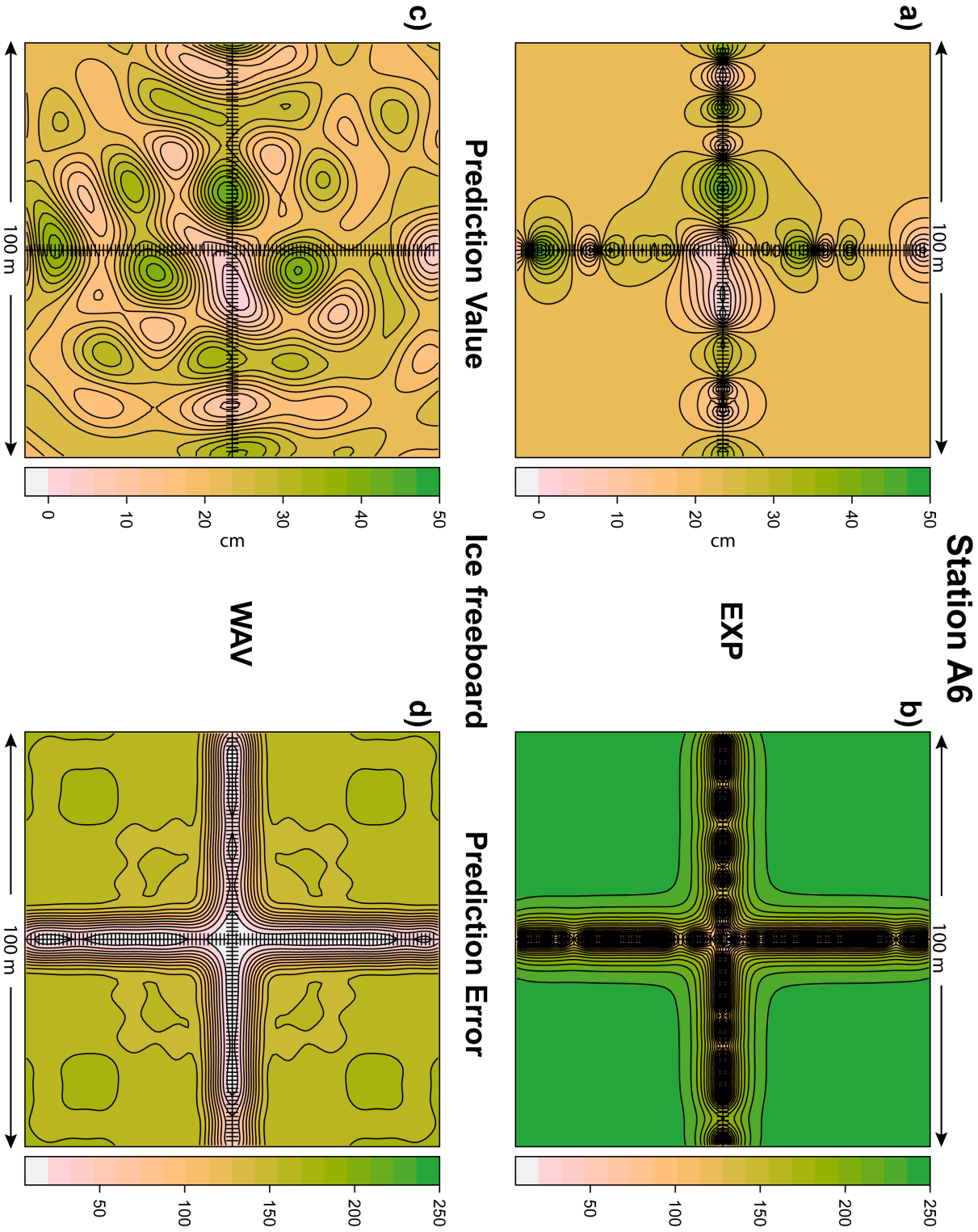

Figure 3.9: Maps with Ordinary Kriging results for sea ice freeboard at station A6: a) Exponential model predicted value, b) Exponential model predicted error, c) Wave model predicted value, d) Wave model predicted error.

3.2.3 Ice thickness and ice freeboard at station A2

The Kriging results of the Wave model from ice freeboard at station A2 varies between 8,7 cm and 16,9 cm with a mean of 11,9 cm (Table 3.1). The total sea ice thickness varies between 164 cm and 185 cm with a mean thickness of 175 cm. These values differ from the observed data, but the mean values and the IQR range of 2,44 cm for the sea ice freeboard and 3,3 for the total sea ice thickness indicate, that the value distribution is similar to the observed distribution. The Kriging settings for these interpolations are described in chapter 3.3. The IQR of the wave model prediction shows that the sea ice thickness has a variable distribution such as it has been the case with the observations of the snow. Nevertheless, the values of the spatial distribution of all estimated data points on the map (Figure 3.4, Figure 3.5 and Figure 3.6) lead to the assumption that there is a relationship between the snow and the sea ice thickness. Lange (2016) showed a negative correlation between the sea ice freeboard and the snow thickness, which is also reflected in the results of the Kriging. The sea ice freeboard values of the whole area are interpreted to reflect the strength and amount of the overlying snow pack that pushes the sea ice surface down. This assumption seems to be consistent with the Kriging results of the snow (Figure 3.5) and therefore supports the sketch of the assumed snow distribution in Figure 3.3. In addition, the relatively thin sea ice close to the centre of the map (Figure 3.4) indicates that there is a lower elevation melt pond, which may also have lower freeboard due to the heavy, thick snow pack pushing the sea ice surface slightly downward in comparison to adjacent sea ice. The modification to the sea ice freboard would be substantially smaller than on FYI station A2 due to the thicker sea ice at MYI station A6. Beyond that, it does show in its overall distribution different grades of thickness than the sea ice freeboard does. This observation can be linked to locally different sea ice growth rates controlled by the thermal insulation of the overlying snow (i.e., more snow has higher thermal insulation and lower ice growth rates resulting in thinner sea ice). This is consistent with results from Lange (2016), who found a negative correlation between snow depth and sea ice thickness and also attributed this to the thermal insulation of snow.

3.2.4 Ice thickness and ice freeboard at station A6

The Kriging results of the Wave model for ice freeboard at station A6 varies between 0.3 cm and 43,6 cm with a mean thickness of 22 cm (Table 3.1). The sea ice thickness varies between 181.14 cm and 353 cm with a mean thickness of 277,5 cm. These values differ from the observed data. The mean values and the IQR of 6,7 cm for the sea ice freeboard and 39,4 for the total sea ice thickness indicate, that the value distribution is not similar to the observed distribution. The Kriging settings for these interpolations are given in chapter 3.2. The IQR of the Wave model prediction shows that the sea ice thickness appears to have an undulating distribution such as it has been the case with the observations of the snow. Nevertheless, the values of the spatial distribution of all

estimated data points on the map (Figure 3.7 and Figure 3.9) lead to the assumption, that there is a relationship between the snow and the sea ice thickness. Lange (2016) showed a negative correlation between the sea ice freeboard and the snow thickness, which is also reflected in our results of the Kriging. The sea ice freeboard values of the whole area show a mix of hummocky and channelized features, whose elevations do mainly match the values of the snow Kriging. This means that areas with high sea ice freeboard (i.e., higher ice topography) values do have a thinner snow cover on it and vice versa. Therefore, it also supports the sketch of the melt ponds and previous summer(s) melt channel systems that was done by looking on the snow elevations (Figure 3.3). Furthermore, it turned out that there is probably a new or relatively young refrozen melt pond close to the centre of the map on top of a hummock, which is only covered by a thin layer of snow (Figure 3.8 and Figure 3.9). The high overall sea ice thickness may indicate, that the observed area is located within stable conditions for sea ice, which supported its growth, even if it was obviously thinning a bit out at some locations by melting events during previous summer(s), e.g. the low spots close to the centre of the map or in the very north of the data cross in Figure 3.7.

3.3 The Variogram

The experimental sample semivariograms were calculated for each property of each station. It is defined as the average degree of dissimilarity between unsampled and nearby data and can show autocorrelations at different distances (Deutsch & Journel, 1998). For a given distance of h, the value is half the average squared difference between $z(u_i)$ and $z(u_i + h)$ (Deutsch & Journel, 1998):

$$\acute{\gamma}(h) = \frac{1}{2N(h)} \sum_{i=1}^{N(h)} [z(u_i) - z(u_i + h)]^2 \tag{3.1}$$

where $N(h)$ is the number of points within the given distance class and direction (Robinson & Metternicht, 2006). Based on these values, 15 semivariance measurements were calculated equally over an Euclidian distance of 50. This approach is also known as the "classic" sample semivariogram (Journel & Huikbregts, 1978).

By looking at the semivariograms presented in Figure 3.10 - Figure 3.13 it is apparent that all snow and sea ice properties at each station display a irregular cyclical pattern, which is a typical pattern for a hole-effect in a semivariogram model. The hole-effect is given when there is a non-monotonic growth of the ordinary least squares estimations in the semivariograms, which presents peaks and valleys (Journel & Froidevaux, 1982). Since our data are three-dimensional, we decided to build up a unique omnidirectional, experimental 3d model. The equation is given in chapter 2.2.1.

A common solution is to ignore the complexity of a cyclical semivariogram and fit the experimental sample semivariogram by using a Spherical or Exponential model through

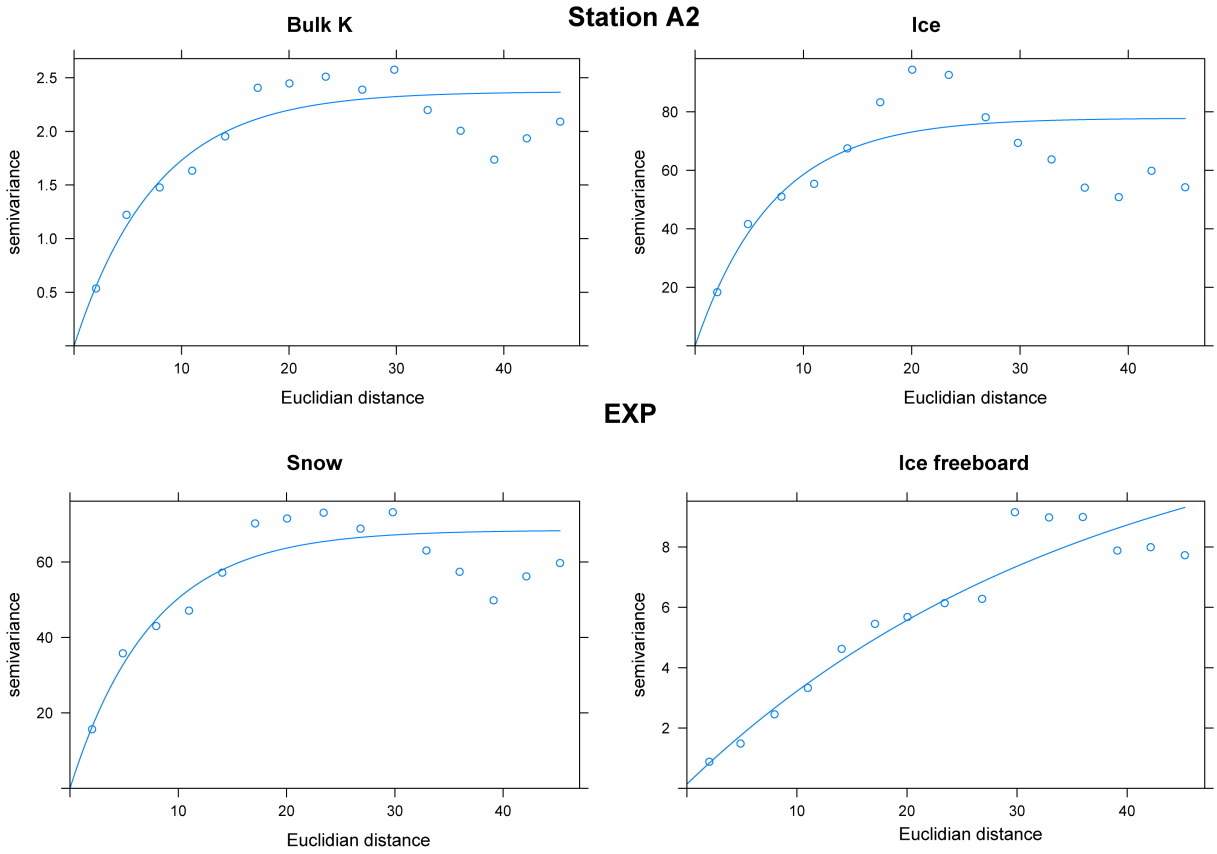

Figure 3.10: Semivariogram of each property at station A2 using the Exponential model

the peaks and troughs (Journel & Froidevaux, 1982). Journel & Froidevaux (1982) pointed out that neglecting the hole-effects is caused by the assumption of high uncertainty at the

peaks and troughs, because of missing data, but could also be caused by representing real topographic features of the property. Since there is no measurement lag in the data, we expect that the data describe particular features of the snow and ice properties. The hole-effects of our data are not related to high uncertainty at the peaks and troughs. In the case that the properties are showing a real cyclical patter, this needs to be accounted for to representatively model and interpolate the property. Since one objective of this study is to reproduce the three dimensional local variations of the snow and sea ice properties, which are known to show some cyclical patterns (e.g., Gosselin et al., 1986), we used the Wave model (i.e., a type of hole-effects model) in combination with the Exponential model; and compared the results. The characteristic cyclical pattern of the Wave model (i.e., hole effects) semivariograms (Journel & Froidevaux, 1982) for the snow and sea ice properties (Figure 3.10 - Figure 3.13) do reflect the typical undulating snow and sea ice topography, such as snow drifts (Gosselin et al., 1988), and MYI hummocks and refrozen melt ponds (Perovich et al., 2003; Sturm et al., 2003). In addition, the Exponential model was chosen to show for comparison the behaviour of an asymptotic and more commonly used function in semivariogram modelling and Ordinary Kriging.

As previously mentioned, the theoretical variogram models (chapter 2.2.1) were built up

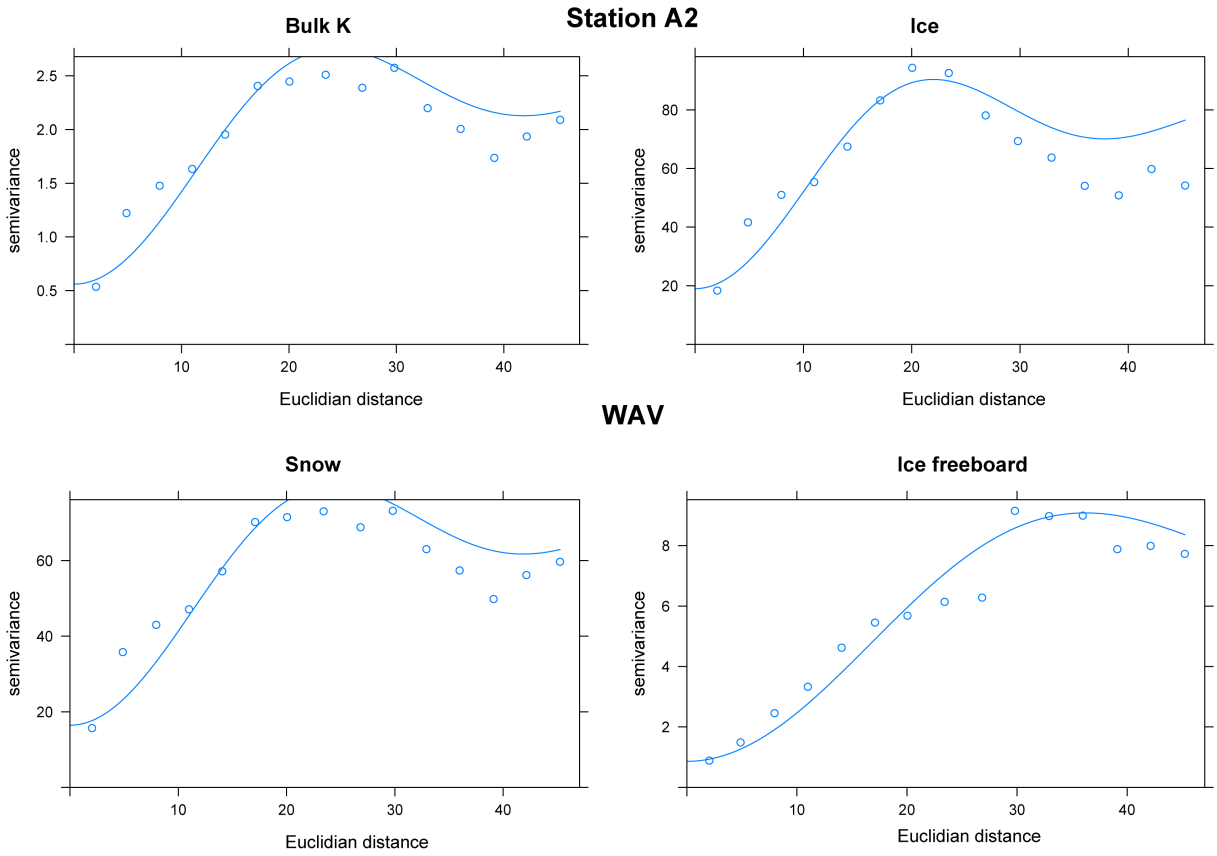

Figure 3.11: Semivariogram of each property at station A2 using the Wave model

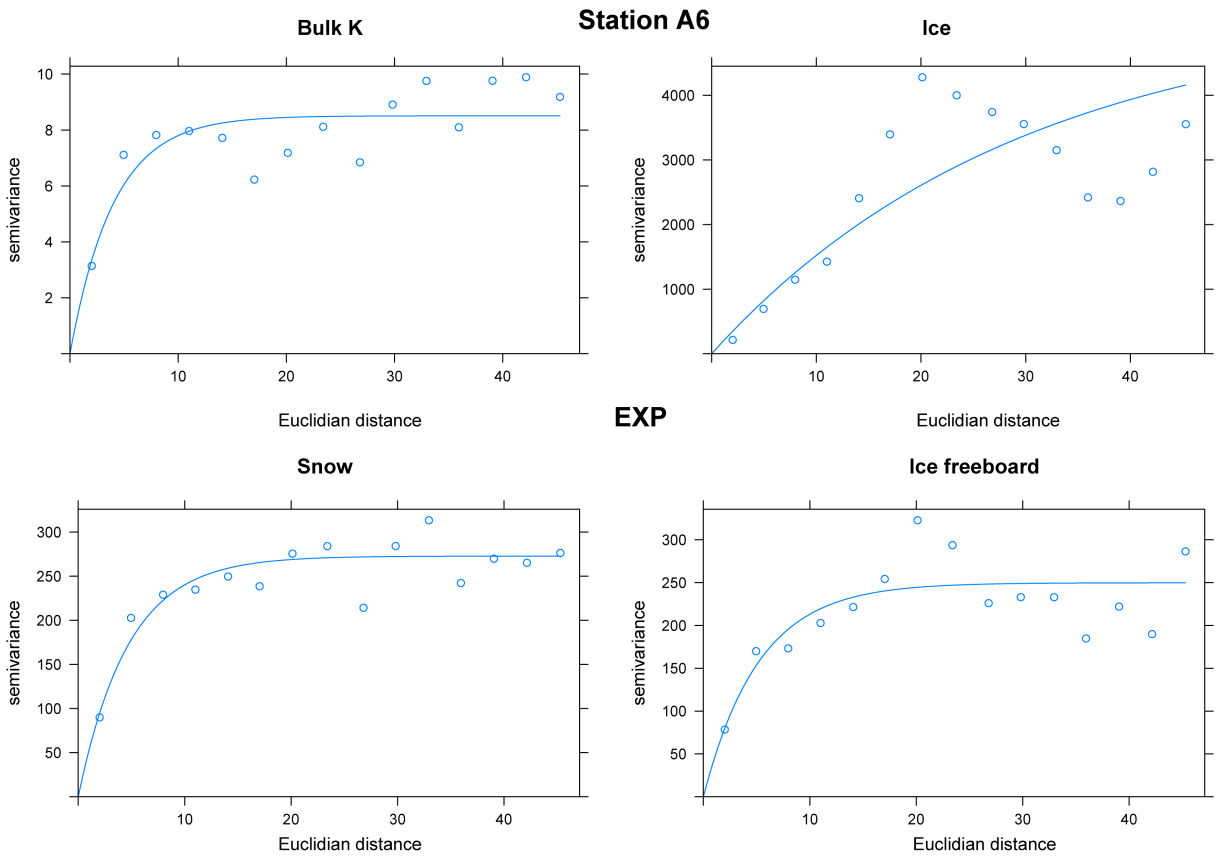

Figure 3.12: Semivariogram of each property at station A6 using the Exponential model

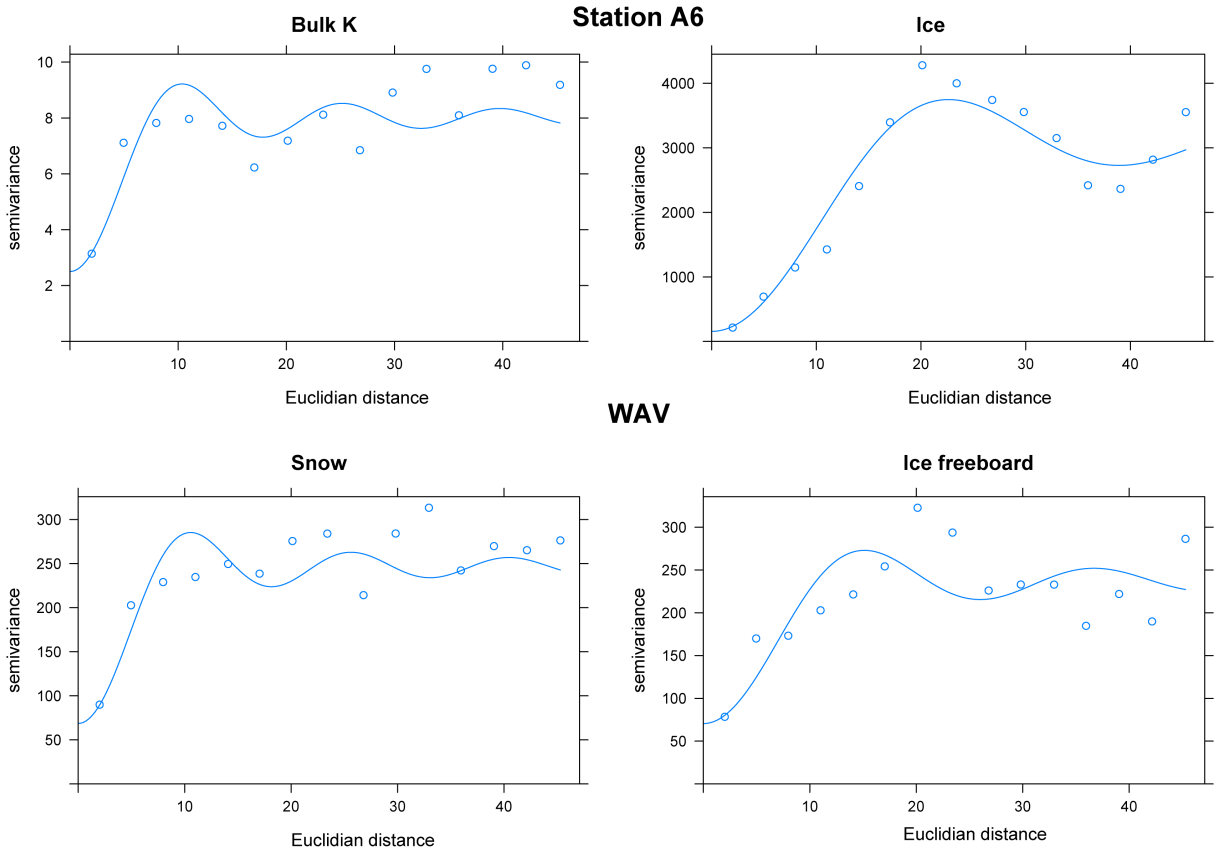

Figure 3.13: Semivariogram of each property at station A6 using the Wave model

with two different model types, the Exponential model and the Wave model. The single values of the partial sill, the partial range and the nugget are shown in Table 3.2 for each station and each model. The workflows for calculating the sill, the range and the nugget are presented in chapter 2.2.1. Fitting the experimental sample semivariogram proportional to the theoretical model was approached by the following weighting (Journel & Huikbregts, 1978):

$$\frac{N(h)}{h^2} \tag{3.2}$$

Where $N(h)$ is the number of point pairs at its distance interval h. The iterative procedure did not guarantee an overall perfect estimation by non-linear estimation. It turned out that a suitable initialisation of the parameters – nugget, sill and range – did not produce the best fit. Therefore, each fit experiment was checked by looking on a common plot of the experimental sample semivariogram and the theoretical model. The results of the best fits are presented in Figure 3.10 - Figure 3.13 and their parametrizations are shown in Table 3.2. Those best fits were used to conduct the Ordinary Kriging interpolation analyses (Chapter 3.4). By looking at the fitted variogram models (Figure 3.10 - Figure 3.13), it is apparent from a visual inspection that the amplitudes of the Wave models describe the overall undulating cyclical pattern of the sample variogram better than the Exponential model.

The variograms of the Bulk K, sea ice thickness, sea ice freeboard and the snow depth at station A2 show a slightly better fit using the Exponential model than the Wave model

in the short Euclidian distances between 10 – 20 (Figure 3.10). At the large distances, 20 m – 50 m, the Exponential model levels at approximately the sill value, however, never reaching it since it is an exponential function (Figure 3.10). The Wave model has a slightly poorer fit at the short lag distances (2 - 20) compared to the Exponential model for the K bulk, the sea ice and the snow, however, the Wave model shows a much better fit at the large distances 20-50 (Figure 3.10 and Figure 3.11). Modelling and fitting the sea ice freeboard (i.e., the sea ice surface) was a bit difficult, because it grows more or less monotonic with small irregular hole-effects and shows then a strict hole-effect at the lag distance of around 38 – 40 (Figure 3.10 and Figure 3.11). Therefore, a large range had to be set for both models. Both models produced a gentle overestimation of the data, but the overall progression was also reached slightly better by the Wave model. The sample variograms of site A2 do represent the more constant spatial thickness distribution of the sea ice properties than it can be seen in the sample variograms of station A6. The sample variograms of station A6 do show a higher variation of the periodicity (Figure 3.12 and Figure 3.13), which more accurately represents the highly undulating and hummocky topographical surface features of MYI (Perovich et al., 2003). On the lag distance between 0 and approximately 9 the Exponential model provides a better fit (Figure 3.12). However, the amplitude of the Wave model estimates the overall cyclical pattern better even if it still overestimates and underestimates at some distances along the sample semivariogram (Figure 3.13).

3.4 Ordinary Kriging

The data implementation of the Ordinary Kriging was approached in two steps. First the settings of the theoretical models were calculated by fitting them to the sample semivariograms of the original data sets. To validate the estimation performance of the Ordinary Kriging method by using two different models, we used a second step: we took a random sample of 100 data points from the 201 total measurements to use for the Ordinary Kriging interpolations. There were always different random samples taken for each station, because we wanted to focus on the general accuracy skills of the models and not on reaching the same accuracy for the same coordinates at each station. Range, nugget and sill were set by using the value calculations of the observed data (Table 3.2). The total data sets of each property at each station, which were not used for the Ordinary Kriging procedure, were stored as well to compare and measure the accuracy of the estimation afterwards. Ordinary Kriging estimated 10609 data points for each property on a given grid with an overall dimension of 100 m x 100 m. The size of a single grid cell was set to 1 m x 1 m. The comparison of the Kriging values at each given sample location with the original value was done by calculating several statistical metrices. First we calculated for each location with a reference value in the observed data set the single error value (SEV)

Table 3.2: Summary of the settings for the theoretical variogram for each station and each property. R = Range; S = Sill; Ng = Nugget

ST	**P**	**Mdl**	**R**	**S**	**Ng**
A2	BK	Exp	10	2,1021	0,5493
A2	I	Exp	10	63,957	21,207
A2	S	Exp	10	60,546	16,2375
A2	IF	Exp	44	7,9345	1,4137
A2	BK	Wav	18	2,1021	0,5493
A2	I	Wav	15,5	63,957	21,207
A2	S	Wav	18	60,546	16,2375
A2	IF	Wav	26	7,9345	1,4137
A6	BK	Exp	12	9,2356	3,4539
A6	I	Exp	7	2821,2	232,45
A6	S	Exp	7	295,24	102,789
A6	IF	Exp	7	234,95	90,8664
A6	BK	Wav	8,5	9,2356	3,4539
A6	I	Wav	15	2821,2	232,45
A6	S	Wav	9	295,24	102,789
A6	IF	Wav	12	234,95	90,8664

Table 3.3: Statistical summary of the Error value distribution from the Ordinary Kriging for each station and each property. P= Property; St = Statistical metric; ST Mdl = Station & Model (e.g., A2/EXP = station/model).

P	**St / ST & Mdl**	**A2/EXP**	**A2/WAV**	**A6/EXP**	**A6/WAV**
BK	Min	0,07555	0,04443	0,296	0,3106
BK	IQR	0,96059	1,27299	1,458	0,8864
BK	Mean	2,50461	1,58905	10,044	6,5529
BK	Max	3,19454	2,43261	11,425	8,0603
I	Min	1,662	1,573	30,46	15,83
I	IQR	26,032	35,144	1777,22	1376,36
I	Mean	81,7	52,837	2635,41	1986,68
I	Max	100,839	78,144	4116,95	2992,01
S	Min	2,117	1,305	8,819	8,869
S	IQR	26,472	36,599	64,138	38,449
S	Mean	72,405	45,847	336,858	223,261
S	Max	91,48	70,16	391,096	284,696
IF	Min	0,1728	0,05503	7,42	7,06
IF	IQR	5,5904	6,54144	41,9	43,05
IF	Mean	6,7706	4,73394	262,24	169,73
IF	Max	12,3807	8,67396	300,29	223,84

as being the difference between the predicted and the observed value:

$$SEV = z(e_i) - z'(e_i) \tag{3.3}$$

where $z(e_i)$ is the Ordinary Kriging estimated value and $z'(e_i)$ the observed value not included in the Ordinary Kriging estimation (i.e., the 100 measurements not included in the Ordinary Kriging interpolation). These values were then used to calculate the mean error (BIAS), the squared sum of the single errors (SSE) and the root mean squared error (RMSE) by the given equations:

$$BIAS = \sum_{i=n}^{N} \frac{\{z(e_i) - z'(e_i)\}}{N} \tag{3.4}$$

$$SSE = \frac{1}{N} \sum_{i=n}^{N} \{z(e_i) - z'(e_i)\}^2 \tag{3.5}$$

$$RMSE = \sqrt{\frac{1}{N} \sum_{i=n}^{N} \{z(e_i) - z'(e_i)\}^2} \tag{3.6}$$

where N is the number of values. The results are given in Table 3.1. The RMSE values do show that the Exponential model has a bit better accuracy than the Wave model for all observed properties. These differences, however, are relatively small compared to the actual values (i.e., 100 measurement points not used in the Ordinary Kriging analyses). Since the Kriging method is based on a best linear unbiased estimator (BLUE, chapter 2.2) the given BIAS values reflect an estimate from an unbiased estimator. Although the BIAS is a random BIAS, for the K bulk calibration it was caught very well (Table 3.1) by both models. The calibration of the sea ice freeboard at station A2 was also very good. However, the BIAS of the sea ice thickness at station A6 estimated by the Exponential model displays a bad result, while the same occurs at the snow thickness at station A6 by using the Wave model. The other properties of both stations indicate to moderate BIAS values (Table 3.1).

On the contrary, the prediction error maps of all observed properties from both stations (Figure 3.4 - Figure 3.9) show that the Wave model always has smaller error values than the Exponential model. The error values level out in an asymptotic way similar to as it was observed previously on the spatial distribution of the prediction values (chapter 3.1). The prediction error maps of the Wave model also level out, but in a more cyclical way (i.e., dampening of the cycles), which might be responsible for the lower error value, because it is not aspire against a certain value and shows still variations instead, even they are not braced that much to the data points anymore.

These results finally point out that the Exponential model fits and estimates data at the short distances better than the Wave model, because at the short distances the sample semivariograms do show mainly a more asymptotic progression than a periodic pattern

(Figure 3.10 - Figure 3.13). This likely had a higher impact on the results of the statistical analysis because the hold-out points (i.e., 100 measurements not used in Ordinary Kriging) were likely in close proximity to the points used for Ordinary Kriging interpolation. On the other hand, the maps of the prediction errors (Figure 3.4 - Figure 3.9) and their value distributions (Table 3.3) indicate that for higher topographical and spatial variations, such as it has been observed on the MYI at station A6, the Wave model may produce a more representative snow and ice surface by capturing the real cyclical the patterns of the snow and sea ice features better than the Exponential model. For sea ice with a more level spatial distribution, such as the FYI of station A2 with a less pronounced cyclical pattern, simple models such as the Exponential model may provide a similar fit and estimate the larger patch sizes (i.e., peaks and troughs) equally good in comparison to the Wave model. For MYI with much larger variability in magnitude and on smaller spatial scales of all properties, which is apparent from the higher frequency and amplitudes of the MYI sample semivariograms (Figure 3.10 - Figure 3.13), the Wave model is superior than a simple model such as the Exponential model.

Chapter 4

Discussion

The main outcome of chapter 3.1 and chapter 3.2 is, that as every model and method with a theoretical and statistical background such as it was performed in this study by using Ordinary Kriging with a hole-effect model cannot estimate the exactly observed prediction range, but it can confirm assumptions of the main surface topography such as snow drift and melt ponds, that were made by looking only on to the observed data.

For station A6, the MYI station, it confirms that the accumulation of water in low spots during summer (e.g., melt ponds) results in enhanced melt in these locations, due to increase solar absorption, compared to the adjacent white ice. This process results in differential melt rates between white ice and melt ponds, which creates high elevation spots (e.g., hummocks) and low elevation spots (e.g., melt ponds). This process would cause even larger ice thickness differences between hummock ice and melt pond, by further exasperating the differential melt by inducing differential growth, i.e., more growth at low snow hummocks due to less thermal insulation and less growth in areas of high snow accumulation such as melt ponds.

For station A2, the FYI station, it confirms that the snow accumulation can be mainly controlled by wind transport which results in a widespreaded surface cover of snow drifts.

Observations by Pyrcz & Deutsch (2003) tell us, that all semivariance values above the sill are negative correlated between their locations. This pattern of negative correlation does exist in all data sets used in this study (Table 3.1, Figure 3.5 - Figure 3.9) and therefore also confirms the negative correlations between the properties that has already been observed on these data by Lange (2016).

The aim of fitting the experimental model by adding a theoretical model such as the Exponential model and the Wave model was to capture the actual pattern of the data in any direction and to satisfactorily produce a realistic snow and sea ice matrix in three dimensions, which also accurately captures important features of the sea ice such as hummocks, snow drift patterns and interconnected melt pond systems. It turned out that using Ordinary Kriging provided by an Exponential model produces a surface that is heterogenic and does not represent the (spatial) variability of the snow and ice properties. It ignores the uncontinuously growth of the experimental variogram and therefore seems

to be unrealistic. Against that the Wave model seems to be more effective and realistic, because it considers those irregularities in the experimental variogram.
This study also shows, that the Wave model can estimate results better for the main objective of this study, even when these results in comparison to the Exponential model are not supported by the statistical outcome such as RMSE or BIAS. In addition I think a more spacious distribution of the measurements could improve the results.
Using sinusoidal, isotropic second order stationary models for (Ordinary) Kriging is still an underrepresented topic of performing geostatistical interpolation and there are less studies published using those methods such as Das, Subba Rao & Boshnakov (2012). Journel & Froidevauy (1982) have already noticed it 34 years ago and suggest that it is caused by its internal complexity. Modelling with a hole-effect model should get much more attention in the field of sea ice research and in general.
It has the potential to become a very useful and supportive tool for estimating the spatial patch size of habitats for ice algae and other members of the Arctic ecosystem within a scale of 100 m x 100 m such as it has been done for this study, but it still needs to be further tested wether other scales can be applied as well.
This study has shown that Ordinary Kriging as a method itself and the way of modelling with Ordinary Kriging might be the best for the spatial variability of snow and sea ice properties, but it needs to be developed furher. There are several opportunities such as using Universal Kriging, trying other hole-effect models or combining two different hole-effect models that need to be implemented and tested in particular. It is also necessary to test those different approaches with many data sets of snow and sea ice properties from different environmental areas and different distribution patterns of the measurement points to verify the chosen way of thinking, to find out, which measuring pattern of the snow and sea ice properties produces the most reliable prediction. It also has to be considered how and if other features of sea ice such as polynyas can be reproduced in those models. Another way could be to sample a few data sets from FYI floes and MYI floes within a regular sampling interval of 1 – 2 m over an area of 100 m x 100 m. Those data sets could be used to test, train and optimize Ordinary Kriging modelling for the aims of this study. Furthermore, it should be used to implement and test other modelling methods from the non-statistical and the statistical families such as Inverse Distance Weighting Interpolation, Nearest Neighbour Interpolation or Universal Kriging, by extracting different measurement patterns from those data sets. However, sampling those training data sets is very time consuming. Nevertheless in my opinion the best verification is still our own background and knowledge of the matter, sea ice and snow, if those methods can be used for our objectives.

Chapter 5

Conclusion

Ordinary Kriging with using hole-effect models appears to be the most realistic way to reproduce and estimate the spatial variability of the snow and ice properties. Using the Wave model can confirm and develop for both stations on a three dimensional scale most of the previously observed variability and relationships between the snow and sea ice properties, but not within the exactly observed prediction range.
The Wave model – and probably further hole-effect models – has the potential to estimate the spatial patch size of habitats for ice algae and other members of the Arctic ecosystem on different spatial scales.
The Exponential model does not produce a surface and estimates a prediction range that represents this variability. It is assumed that similar models such as the Spherical model would perform in a similar way as the Exponential model does. The better results of the Exponential model in the statistical analysis cannot be fully explained.
Modelling with a hole-effect model is still an underrepresented topic in geostatistics and should get much more attention.
This study represents a first approach of modelling the spatial variability of snow and sea ice properties, but needs to be developed further.

Bibliography

[1] The cryosphere today, 2016.

[2] J. J. Cassano, A. DuVivier, M. Hughes, A. Roberts, M. Brunke, A. Craig, B. Fisel, W. Gutowski, W. Maslowski, B. Nijssen, et al. Modeling arctic climate with a regional arctic system model (rasm). *21st Century Challenges in Regional Climate Modelling*, page 10, 2013.

[3] S. Das, T. S. Rao, and G. N. Boshnakov. On the estimation of parameters of variograms of spatial stationary isotropic random processes. Technical report, Technical report, School of Mathematics. The University of Manchester, 2012.

[4] J. Francis. Wacky weather and disappearing arctic sea ice: are they connected, 2013.

[5] M. Gosselin, L. Legendre, J.-C. Therriault, S. Demers, and M. Rochet. Physical control of the horizontal patchiness of sea-ice microalgae. *Mar Ecol Prog Ser*, 29(3):289–298, 1986.

[6] A. Journel and R. Froidevaux. Anisotropic hole-effect modeling. *Journal of the International Association for Mathematical Geology*, 14(3):217–239, 1982.

[7] A. G. Journel and C. J. Huijbregts. *Mining geostatistics*. Academic press, 1978.

[8] C. Katlein, M. Fernández-Méndez, F. Wenzhöfer, and M. Nicolaus. Distribution of algal aggregates under summer sea ice in the central arctic. *Polar biology*, 38(5):719–731, 2015.

[9] B. Lange. *Spatial variability of Arctic sea ice algae*. PhD thesis, University of Hamburg, 2016.

[10] E. R. Miles, C. M. Spillman, J. A. Church, and P. C. McIntosh. Seasonal prediction of global sea level anomalies using an ocean–atmosphere dynamical model. *Climate Dynamics*, 43(7-8):2131–2145, 2014.

[11] J.-M. Montero, J. Mateu, et al. *Spatial and spatio-temporal geostatistical modeling and kriging*, volume 998. John Wiley & Sons, 2015.

[12] D. K. Perovich, T. C. Grenfell, J. A. Richter-Menge, B. Light, W. B. Tucker, and H. Eicken. Thin and thinner: Sea ice mass balance measurements during sheba. *Journal of Geophysical Research: Oceans*, 108(C3), 2003.

[13] M. Pyrcz and C. Deutsch. The whole story on the hole effect. *Geostatistical Association of Australasia, Newsletter*, 18:3–5, 2003.

[14] T. Robinson and G. Metternicht. Testing the performance of spatial interpolation techniques for mapping soil properties. *Computers and electronics in agriculture*, 50(2):97–108, 2006.

[15] A. Rösel, L. Kaleschke, and G. Birnbaum. Melt ponds on arctic sea ice determined from modis satellite data using an artificial neural network. *The Cryosphere*, 6(2):431–446, 2012.

[16] O. Schabenberger and C. Gotway. Spatial methods: for spatial data analysis, 2005.

[17] J. C. Stroeve, V. Kattsov, A. Barrett, M. Serreze, T. Pavlova, M. Holland, and W. N. Meier. Trends in arctic sea ice extent from cmip5, cmip3 and observations. *Geophysical Research Letters*, 39(16), 2012.

[18] M. Sturm, J. Holmgren, and D. K. Perovich. Winter snow cover on the sea ice of the arctic ocean at the surface heat budget of the arctic ocean (sheba): Temporal evolution and spatial variability. *Journal of Geophysical Research: Oceans*, 107(C10), 2002.

[19] A. Swan. Deutsch, cv & journel, ag 1998. gslib. geostatistical software library and user's guide, x+ 369 pp.+ cd-rom. oxford, new york: Oxford university press. price£ 45.00 (hard covers). isbn 0 19 510015 8., 1999.

[20] D. N. Thomas and G. S. Dieckmann. *Sea ice*. John Wiley & Sons, 2009.

Eigenständigkeitserklärung

Assessing the spatial variability of snow and sea ice properties with different spatial analytical approaches

Student:

Vorname: Svenja Annika Nachname: Rudolph

Hiermit erkläre ich, dass die vorliegende Bachelorarbeit von mir selbstständig verfasst wurde und dass keine anderen als die angegebenen Hilfsmittel benutzt wurden. Die Stellen der Arbeit, die anderen Werken dem Wortlaut oder Sinn nach entnommen sind, sind in jedem einzelnen Fall unter Angabe der Quelle als Entlehnung kenntlich gemacht. Diese Erklärung erstreckt sich auch auf etwa in der Arbeit enthaltene Zeichnungen, Karten(skizzen) und bildliche Darstellungen.

Erlangen, 27.9.2016

Ort und Datum

Unterschrift